https://doi.org/10.5194/egusphere-2026-2327
Preprint. Discussion started: 1 June 2026

Contribution of the solar wind-magnetosphere-ionosphere-atmosphere coupling to rapid intensification of tropical cyclones and transition of Mediterranean subtropical cyclones to tropical-like cyclones

Paul Prikryl[1], Vojto Rušin[2]

[1]Physics Department, University of New Brunswick, Fredericton, NB, Canada

[2]Astronomical Institute, Slovak Academy of Sciences, Tatranská Lomnica, Slovakia

Correspondence to: Paul Prikryl (paul.prikryl@unb.ca)

Abstract. We investigate rapid intensification of tropical cyclones and transition of Mediterranean subtropical cyclones to tropical-like cyclones in the context of solar wind-magnetosphere-ionosphere-atmosphere coupling. Using the superposed epoch analysis of time series of solar wind variables, it is observed that rapid intensification of tropical cyclones and transition of Mediterranean subtropical cyclones to tropical-like cyclones tend to occur following arrivals of high-speed solar wind streams from coronal holes or impacts of interplanetary coronal mass ejections. Aurorally generated atmospheric gravity waves can influence the development of weather. While these gravity waves reach the troposphere with attenuated amplitudes, they can contribute to the release of conditional symmetric instability leading to latent heat release and intensification of extratropical and tropical cyclones. We use the meteorological re-analysis to evaluate slantwise convective available potential energy to assess likelihood of conditional symmetric instability that can be released by over-reflecting aurorally generated gravity waves leading to slantwise convection and intensification of storms.

1 Introduction

A tendency of significant weather events, including explosive extratropical cyclones (Prikryl et al., 2009a; 2016), rapid intensification of tropical cyclones (Prikryl et al., 2019), heavy rainfall and flash floods (Prikryl et al., 2018; 2021a,b; Prikryl and Rušin, 2023; Prikryl, 2024), as well as large tornado outbreaks (Prikryl and Rušin, 2025), to occur following arrivals of corotating interaction regions (CIRs) at the leading edge of solar wind high-speed streams (HSSs) from coronal holes and impacts of interplanetary coronal mass ejections (ICMEs), has been documented. Prikryl et al. (2009b) and Prikryl (2024) proposed that aurorally generated atmospheric gravity waves (AGWs) may play a role in intensification of extratropical cyclones by contributing to the release of conditional symmetric instability (CSI) (Schultz and Schumacher, 1999; Chen et al., 2018). Low-level southerly winds and vertical wind shears are favourable conditions for over-reflection of globally

https://doi.org/10.5194/egusphere-2026-2327
Preprint. Discussion started: 1 June 2026

propagating aurorally excited gravity waves that can reach the troposphere and contribute to conditional symmetric instability release leading to slantwise convection.

The solar wind coupling to the magnetosphere–ionosphere–atmosphere (MIA) is most impactful when ICMEs (Burlaga et al., 1981; Gopalswamy, 2016), or HSSs/CIRs from coronal holes (Krieger et al., 1973; Smith and Wolfe, 1976; Tsurutani et al., 1995), interact with the magnetosphere. It is the southward component of the interplanetary magnetic field, often due to solar wind Alfvén waves (Tsurutani et al., 2018), that causes magnetic reconnection (Dungey, 1961, 1995) and solar wind energy input into the magnetosphere and ionosphere. Rather than continuous, the magnetic reconnection is often intermittent or pulsed (Trattner et al., 2015), and the observed ionospheric signatures are known as pulsed ionospheric flows driven by electric fields (Milan et al., 2000; McWilliams et al., 2001). Because of the Joule heating and Lorentz forcing in the ionosphere, a key component of the solar wind coupling to the magnetosphere-ionosphere-atmosphere (MIA) is the generation of AGWs in the lower thermosphere at high latitudes (Hines, 1965; Chimonas and Hines, 1970; Hocke and Schlegel, 1996). The global excitation and propagation of these AGWs in the atmosphere, including the lower atmosphere, where they can be ducted to reach low latitudes, have been demonstrated using a transfer function and raytracing methods (Mayr et al. 1984a, 1984b, 2013; Prikryl et al. 2018; 2019).

Forecasting rapid intensification of tropical cyclones defined as the maximum sustained wind increase of ≥ 30 kt in 24 hours remains a major challenge (Kaplan et al., 2010; DeMaria et al., 2014; 2021; Horinouchi et al., 2025). In the subtropical region of the Mediterranean Sea cyclonic storms occasionally develop into Mediterranean Tropical-Like Cyclones (TLCs), or medicanes (MEDIterranean hurriCANES; Emanuel, 2005). They have been extensively studied (e.g., Real and Atlas, 2001; Miglietta et al., 2013, 2015, 2017; Borzì et al., 2025; Dafis et al., 2020), because they can have significant, sometimes catastrophic, impact in this region (Diakakis et al., 2023).

The aim of the present work is to investigate rapid intensification of tropical cyclones and transition of Mediterranean subtropical cyclones to tropical-like cyclones in the context of solar wind-magnetosphere-ionosphere-atmosphere coupling, to provide further evidence of the link between space weather and tropospheric weather.

2 Data and methods

The revised HURDAT2 database (http://www.nhc.noaa.gov/data/) of “best tracks” of tropical and subtropical cyclones for the Atlantic and East Pacific basins is provided by the National Hurricane Center (NHC) post-storm analyses of the storm intensity (maximum sustained wind in kt), central pressure in mbars (mb), position, and size for every synoptic time (0000, 0600, 1200, and 1800 UTC) (Landsea and Franklin, 2013). The best tracks are smoothed and do not precisely recreate a storm's history, and thus variations over periods shorter than about 24h are typically not captured. These data are used to obtain storm intensity changes in the maximum sustained wind in kt for last 24h. The U.S. government website Joint Typhoon Warning Center (JTWC) is hosted by several agencies including National Oceanic and Atmospheric Administration (NOAA) and National Weather Service (NWS). The products and services include the Tropical Cyclone Best

https://doi.org/10.5194/egusphere-2026-2327
Preprint. Discussion started: 1 June 2026

Track Data http://www.metoc.navy.mil/jtwc/jtwc.html?best-tracks that cover Southern Hemisphere, Northern Indian Ocean and Western North Pacific Ocean.

Partial lists of Mediterranean tropical-like cyclones have been published (e.g., Miglietta et al., 2013; Tous and Romero, 2013; Nastos et al. 2018; Avenas et al. 2026), and several websites provide archives of Mediterranean storm events (http://meteorologia.uib.eu/medicanes/index.html; https://user.eumetsat.int/resources/case-studies/mediterranean-cyclones-medicanes-2007-2021; https://zivipotty.hu/tcr.html; http://medicanes.altervista.org/; https://user.eumetsat.int/resources/case-studies/mediterranean-cyclones-medicanes-2007-2021#ID-Other-image-source). From these resources, a list of medicane storms dates is compiled.

The hourly reanalysis dataset ERA5 with spatial resolution of 0.25 x 0.25 degree (Hersbach et al., 2020) is a product of the European Centre for Medium-Range Weather Forecasts (ECMWF). Following Chen et al. (2018), indices including convective available potential energy (CAPE), slantwise CAPE (SCAPE), and vertically integrated extent of realizable symmetric instability (VRS; a measure to quantify the "releasable" CSI) are diagnosed, to assess the likelihood of slantwise convection during the intensification of tropical cyclones and development of Mediterranean tropical-like cyclones.

The solar wind data are provided by the National Space Science Data Center (NSSDC) OMNIWeb http://omniweb.gsfc.nasa.gov (King and Papitashvili, 2005). The hourly averages of solar wind velocity, V, the interplanetary magnetic field (IMF) magnitude, |B|, the standard deviation of IMF B_z, σ_{Bz}, and the proton density, n_p, are used to identify CIRs, the stream interfaces between the fast and slow solar wind at the leading edge of HSSs from coronal holes (Tsurutani et al., 2006). The OMNI data also include geomagnetic indices, e.g., the *Dst* index that characterize geomagnetic storms (Gonzalez et al., 1994). A catalogue of near-Earth ICMEs (Richardson and Cane, 2010) has been updated (http://www.srl.caltech.edu/ACE/ASC/DATA/level3/icmetable2.htm).

Measurements of the green coronal emission line intensity at 530.3 nm (Fe XIV) by ground-based coronagraphs from 1939 to 2008 have been merged into a homogeneous coronal dataset (Rybanský, 1975; Rybanský et al., 2001, 2005; Dorotovič et al., 2014; https://www.kozmos-online.sk/). The coronal intensities are expressed in absolute coronal units (ACU) representing the intensity of the continuous spectrum from the center of the solar disk with a width of 1 Å at the same wavelength as the observational spectral line (1 ACU = 3.89 W $m^{-2}sr^{-1}$ at 530.3 nm). The coronal intensity depletions, called coronal holes, are sources of HSSs. The green corona intensity for the solar central meridian is computed by averaging the intensities measured at the east and west limbs (Prikryl et al. 2009a).

The superposed epoch (SPE) method (e.g., Ambrož, 1979) is used to investigate rapid intensification of tropical cyclones and the development of Mediterranean tropical-like cyclones relative to solar wind disturbances.

https://doi.org/10.5194/egusphere-2026-2327
Preprint. Discussion started: 1 June 2026

3 Superposed epoch analysis of solar wind variables keyed to the maximum rapid intensification of hurricanes

Prikryl et al. (2019) observed that rapid intensification of tropical cyclones tends to follow arrivals of high-speed solar wind from coronal holes and/or impacts of ICMEs. These authors used the SPE analysis of time series of solar wind variables (V, |B|, n_p, and σ_{Bz},) keyed to times of the maximum rapid intensification (RI) of tropical cyclones defined as the first highest increase in the maximum sustained wind (MSW) over 24 h that reached or exceeded a given threshold value (Prikryl et al., 2019; their Figures 1 and 2). In Fig. 1, the SPE analysis for hurricanes in East Pacific (EPac), North Atlantic (NAtl), and combined (EPac+NAtl) is extended by 8 more years to 1995-2024 using the key times defined by RI ≥ 30 kt/24 h. The results show patterns of the mean solar wind velocity, V, increasing from minimum before the key time to maximum later, with peaks in the mean magnetic field magnitude, |B|, the proton density, n_p, and the standard deviation, σ_{Bz}, near the key time. The patterns that are similar in the cases of EPac and NAtl hurricanes indicate a tendency of RI of hurricanes to occur following HSS/CIRs or ICMEs. Such patterns become more pronounced for higher RI thresholds (Prikryl et al., 2019).

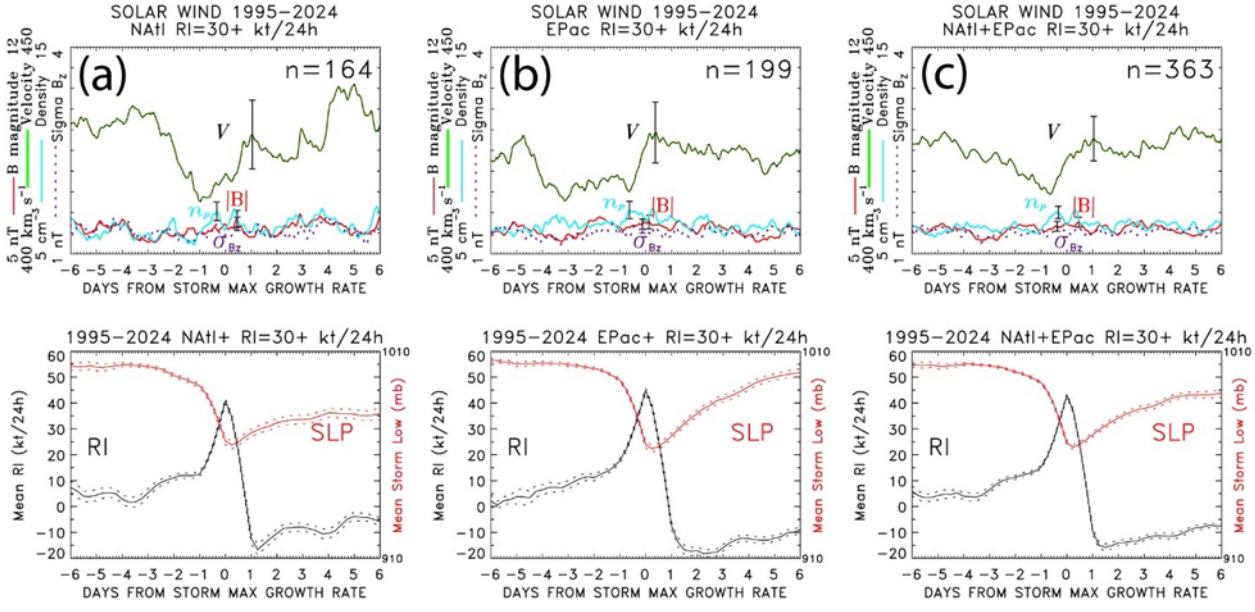

Figure 1: The SPE analysis of solar wind parameters keyed to the first maximum of rapid intensification of 30+ kt/24 h of **(a)** NAtl, **(b)**, EPac and **(c)** Natl+EPac hurricanes. Bottom panels show the mean 6-hourly values of the maximum sustained wind (black lines) and the mean sea level pressure (red lines).

Another way to show this is by defining the key times for the SPE analysis as the actual arrival times of major HSS/CIRs (maximum velocity VMAX > 500 km/s) that were associated with intensifying hurricanes. Fig. 2 shows SPE analysis of

https://doi.org/10.5194/egusphere-2026-2327
Preprint. Discussion started: 1 June 2026

green corona intensity (top panels) and solar wind variables (middle panels) keyed to arrivals of HSS/CIRs that were followed within 3 days by hurricane RI ≥ 30 kt/24h, separately for EPac (Fig. 2a) and NAtl (Fig. 2b) hurricanes, and
120 combined (NAtl+EPac; Fig. 2c). As expected, the superposition of major HSS/CIRs results in clear patterns of the mean velocity V and peaks in |B|, n_p, and σ_{Bz}, at the leading edge of the HSSs from coronal holes. The bottom panels in Fig. 2 show the mean values of the 6-hourly maximum sustained wind (black lines) and sea level pressure (red lines) averaged over the superposed intensifying hurricanes, with histograms showing the number of superposed storms. Some of the superposed HSS/CIRs were followed by RIs of more than one hurricane (EPac or NAtl). These results indicate that about 24% of
125 Natl+EPac hurricanes (87 out of 363) underwent RI ≥ 30 kt/24h (Fig. 1c) following arrivals of major HSSs from coronal holes. This is why the SPE analysis of solar wind variables keyed to times of intensification RI ≥ 30 kt/24h (Fig. 1) reveals the characteristic patterns discussed above.

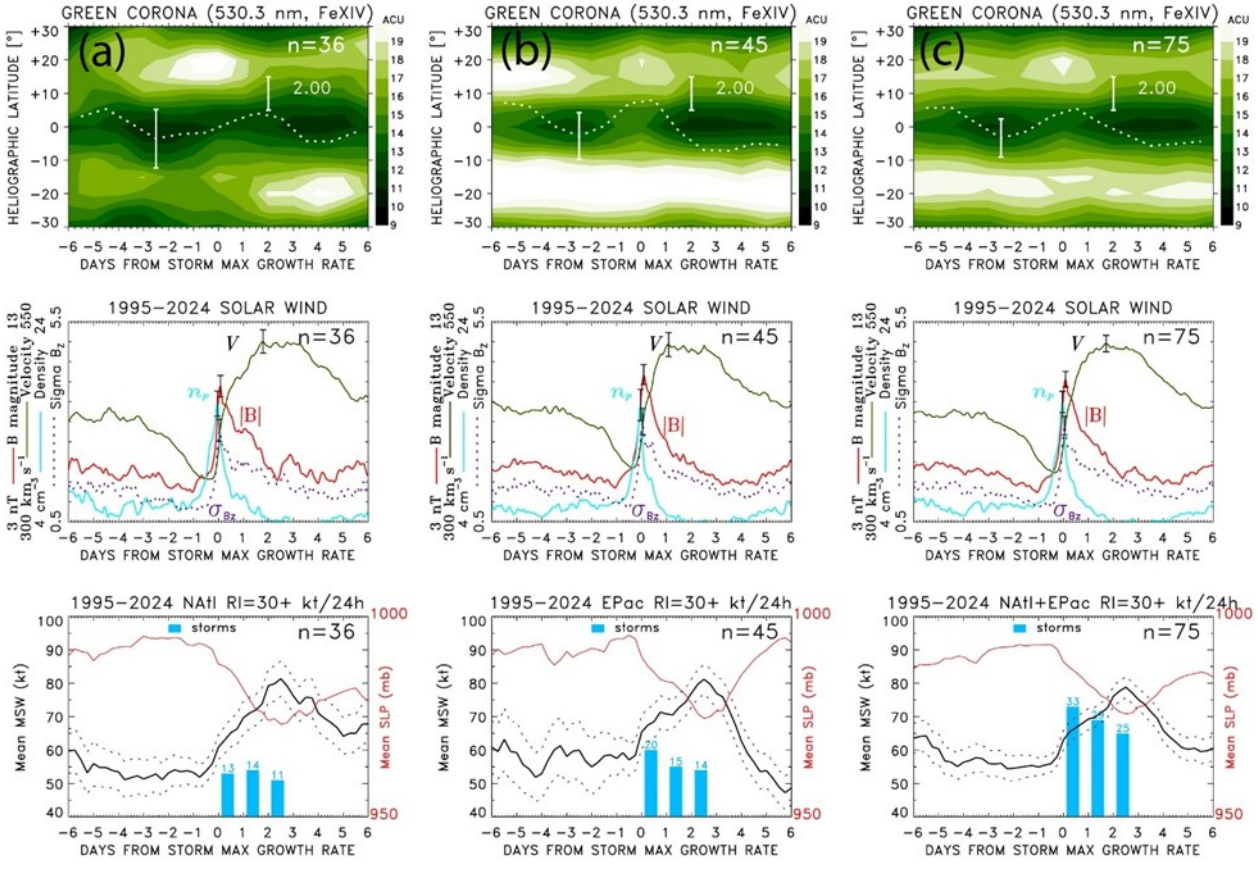

Figure 2: The SPE analysis of time series of green corona intensity, solar wind plasma variables (top and middle panels),
130 and the mean of the 6-hourly values of the maximum sustained wind (black lines) and the mean sea level pressure (red lines) (bottom panels) keyed to arrivals of major HSSs with the maximum velocity VMAX > 500 km/s that were followed within 3 days by RI ≥ 30 kt/24h of **(a)** EPac, **(b)** NAtl, and **(c)** Natl+EPac hurricanes. In the bottom panels, the histograms show the number of hurricanes.

https://doi.org/10.5194/egusphere-2026-2327
Preprint. Discussion started: 1 June 2026

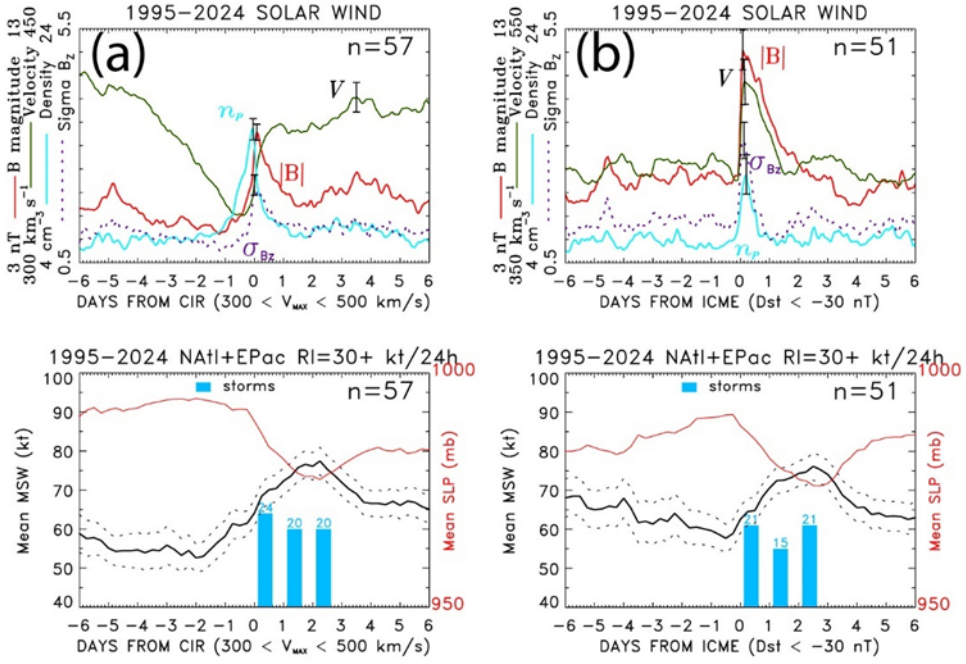

135 **Figure 3:** The SPE analysis of time series of (top panels) solar wind plasma variables and (bottom panels) the mean of the 6-hourly values of the maximum sustained wind (black lines) and the mean sea level pressure (red lines) keyed to **(a)** arrivals of minor to moderate HSSs (300 < VMAX < 500 km/s) and **(b)** impacts of ICMEs, that were followed within 3 days by RI ≥ 30 kt/24h of NAtl+EPac hurricanes. In the bottom panels, the histograms show the number of hurricanes.

140 Furthermore, Fig. 3a shows that another 18% of Natl+EPac hurricanes (64 out of 363) rapidly intensified following minor to moderate HSSs (300 < VMAX < 500 km/s), and Fig. 3b shows that about 16% of Natl+EPac hurricanes (57 out of 363) rapidly intensified following impacts of ICMEs that caused geomagnetic storms (*Dst* < −30 nT). As expected for interplanetary shocks ahead of ICMEs, the mean values of all four solar wind variables sharply increase at the key time. The results in Figs. 2 and 3 support the conclusion that RIs of hurricanes often occur following arrivals of HSSs from coronal
145 holes or impacts of ICMEs (Prikryl et al., 2019). Similar results of the SPE analysis for typhoons can be viewed in the Supplement (Figures S1 and S2).

4 Cases of RI of tropical cyclones in the context of solar wind

Fig. 4 shows the hourly OMNI solar wind data (V, |B|, n_p, and σ_{Bz}) along with the geomagnetic storm index *Dst*. The red
150 asterisks and orange triangles on the time axis indicate arrivals of HSS/CIRs and impacts of ICMEs, respectively. The maximum sustained wind (MSW) (scaled symbols) and RI in 24 h (thin solid lines) from the best track data of major tropical cyclones are shown at the top of each panel.

https://doi.org/10.5194/egusphere-2026-2327
Preprint. Discussion started: 1 June 2026

4.1 Hurricanes Oho, Olaf and Patricia in October 2015

In October 2015, the East Pacific hurricanes Oho, Olaf and Patricia (Fig. 4a) intensified following HSS/CIR arrivals. Hurricane Oho reached the maximum RI > 25 kt/24 h which coincided with a major HSS/CIR that triggered a moderate geomagnetic storm on October 7 as indicated by Dst index. Hurricane Olaf reached the maximum RI >30 kt/24h on October 19, following the arrival of HSS/CIR on October 18 that triggered a weak geomagnetic storm. Hurricane Patricia was an extraordinary tropical cyclone that broke many records, including maximum RI = 105 kt/24h on October 23 (Rogers et al., 2017). It formed and started to intensify with the arrival of HSS/CIR on October 21. This was a structured HSS that originated from multiple coronal holes, with another steep increase in solar wind velocity by the end of October 22 and followed by an ICME 2 days later.

https://doi.org/10.5194/egusphere-2026-2327
Preprint. Discussion started: 1 June 2026

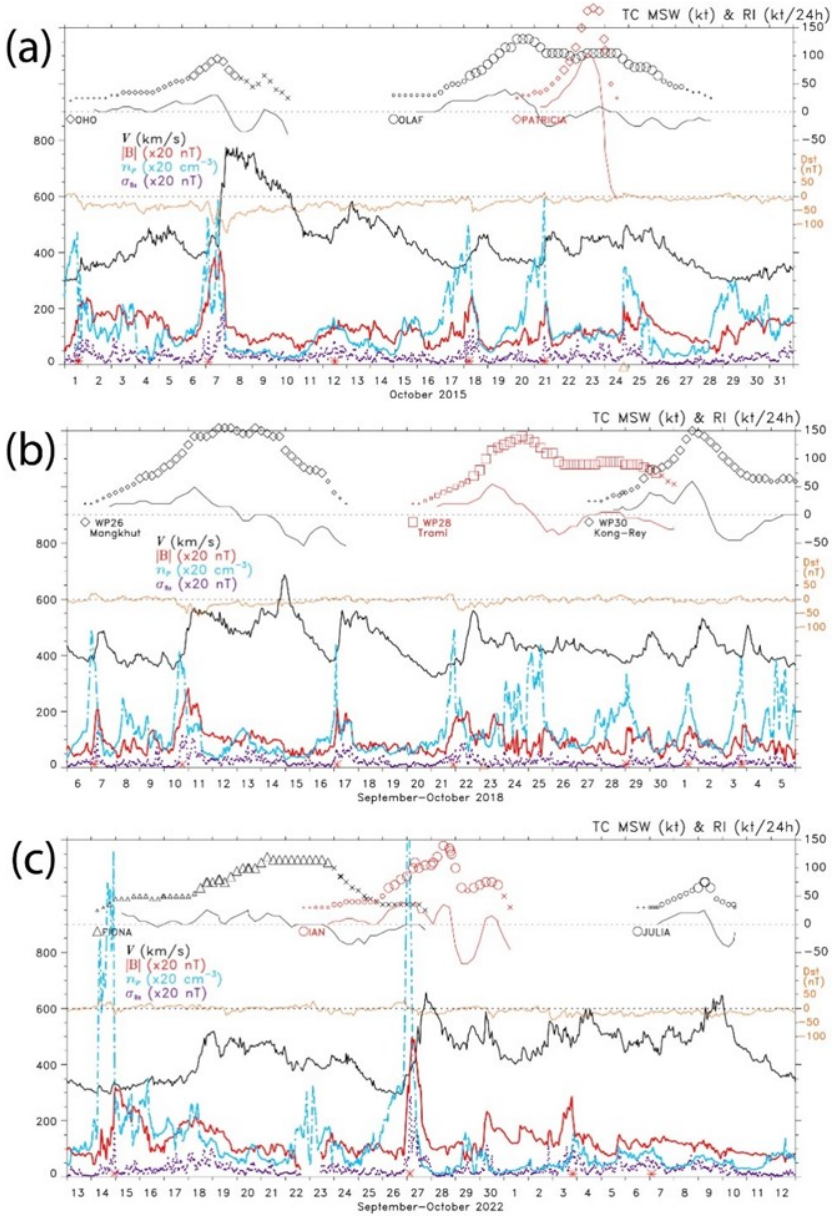

Figure 4: In the bottom half of each panel, the hourly OMNI solar wind data of V (black), **B** (red), n_p (broken light blue) and σ_{Bz} (dotted purple) are shown with the left y-axis scale factors printed. The geomagnetic storm index Dst is also shown (orange line). Red asterisks and orange triangles on the time axis indicate CIRs and ICMEs, respectively. In the top half of each panel, the "best track" data of **(a)** East Pacific hurricanes, **(b)** West Pacific typhoons, and **(c)** North Atlantic hurricanes, with the maximum sustained wind (MSW) (scaled symbols) and RI in 24 h (thin solid lines) are shown. The tropical cyclone names are printed at the initiation time marked with symbols used for each tropical cyclone.

https://doi.org/10.5194/egusphere-2026-2327
Preprint. Discussion started: 1 June 2026

4.2 Typhoons Mangkhut, Trami and Kong-Rey in September-October 2018

In Fig. 4b, the "best track" data of West Pacific typhoons Mangkhut, Trami and Kong-Rey. Super Typhoon Mangkhut had a long lifespan and attained high intensity becoming the most impactful typhoon in 2018 (Huang et al., 2020; Lo et al., 2020). The operational track forecasts showed a great uncertainty, and the forecast landing points varied with different lead times (Huang et al., 2020). Typhon Mangkhut rapidly intensified following the impact of HSS/CIR that triggered a weak geomagnetic storm on September 10. It maintained very high intensity (category 5) for at least 3 days as the Earth was impacted by another strong HSS. It lost some of its power after landing on the northern tip of Philippines but still caused an extraordinary rain event in the Yangtze River Delta region on 16 September (Yu et al., 2020).

Typhoon Trami grew from a tropical storm that rapidly intensified into a typhoon on September 22 following the arrival of HSS/CIR that triggered weak geomagnetic storm. It then briefly reached intensity of a super typhoon category 5 on September 24.

Another super typhoon developed from a tropical depression upgraded to tropical storm on September 28 that intensified to typhoon Kong-Rey following the arrival of a moderate HSS/CIR on September 29. On October 1, Kong-Rey rapidly intensified into a super typhoon with the arrival of a second HSS/CIR.

4.3 Hurricanes Fiona and Ian in September 2022

Fig. 4c shows the "best track" data of the North Atlantic hurricanes Fiona, Ian and Julia. All three hurricanes intensified following HSS/CIR arrivals.

Tropical storm Fiona formed and intensified following the impact of a strong CIR on September 14-15 at the leading edge of an initially relatively slow HSS. With the arrival of a much faster and structured HSS on September 18 Fiona rapidly intensified into a hurricane that continued to intensify as it was passing over the Caribbean Islands. It interacted with a cold front on September 24 and transitioned into an intense extratropical cyclone.

The first RI > 30 kt/24 h of hurricane Ian coincided with a major HSS/CIR that triggered a weak geomagnetic storm on September 26-27. After the second RI it landed in Florida and later transitioned into an extratropical cyclone affecting the eastern U.S. and Canada. Tropical storm Julia formed and intensified into a hurricane following a moderate HSS/CIR on October 7.

5 Convective bursts and tropical cyclone rapid intensification

The role of deep convective processes, including vortical hot towers, contributing to tropical cyclone formation and intensification has been recognized (Hendricks et al., 2004; Sanders and Montgomery, 2004; Montgomery et al., 2006; Hendricks, 2012; Callaghan, 2024). Convective bursts (CBs) preceding, or coinciding with, the onset of RI of TCs have been observed and are considered important in the development of TCs (Steranka et al., 1986; Rodgers et al. 1998, 2000; Price et al. 2009; Guimond et al. 2010; Chen and Zhang, 2013). Fig. 5 shows the GOES-16 infrared (IR) images extracted from

https://doi.org/10.5194/egusphere-2026-2327
Preprint. Discussion started: 1 June 2026

205 SLIDER by RAMMB/CIRA @ CSU (https://rammb-slider.cira.colostate.edu/) during intensifications of hurricanes Fiona and Ian that displayed CBs in September 2022. Hurricane Fiona showed a series of CBs, particularly when it intensified on September 18 as it was passing over the Caribbean Islands (Figs, 5a, b). The IR images (Figs. 5c, d) of hurricane Ian also displayed a series of CBs, while it was intensifying on September 26 and 28.

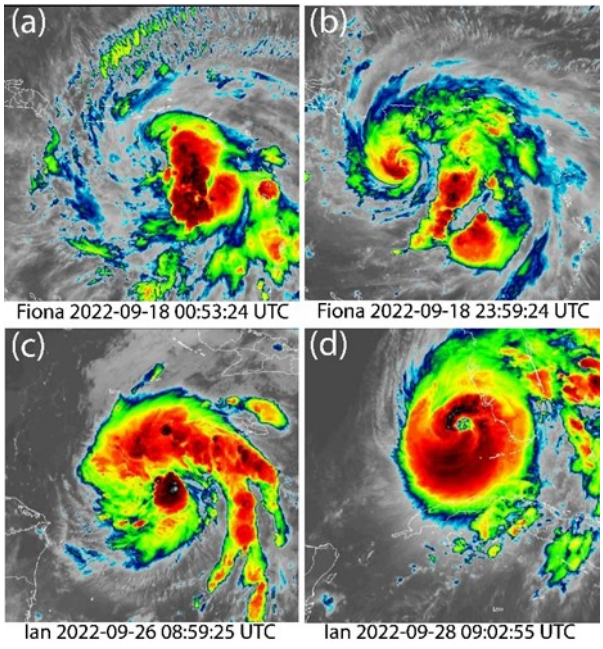

210 **Figure 5:** The GOES-16 IR images (Band 13: 10.4 µm) of hurricane **(a, b)** Fiona and **(c, d)** Ian extracted from SLIDER by RAMMB/CIRA @ CSU animations.

In the context of solar wind, Prikryl et al. (2019) considered cases of TCs that displayed CBs and used SPE analysis of solar
215 wind parameters keyed to intensifications of TCs with CB episodes to show a tendency that RIs of these storms followed arrivals of HSS/ CIRs or ICMEs (see, their Figure 19). Using an extended list of TCs with CBs from 1995 to 2022, the SPE analysis further confirms those results. Fig. 6 shows a clear pattern of the mean solar wind parameters that is consistent with Figs. 1–3, indicating that RIs of many of these storms followed, or coincided with, arrivals of HSS/ CIRs or ICMEs. This is supported by histograms of the occurrence distributions of major HSSs/CIRs and ICMEs that peak just before the key time
220 (Fig. 6c). Similar results for hurricanes and typhoons separately can be viewed in the Supplement Figure S3.

https://doi.org/10.5194/egusphere-2026-2327
Preprint. Discussion started: 1 June 2026

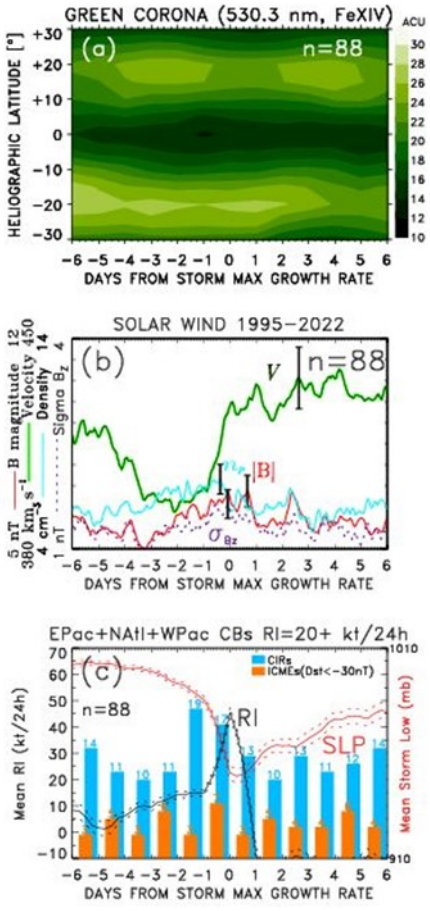

Figure 6: The SPE analysis of (a) green corona intensity, (b) solar wind plasma parameters and (c) SLP and RI keyed to the maximum intensification (RI = 20+ kt) of tropical cyclones with convective bursts (CBs). The histograms of occurrence distributions of major HSSs/CIRs (light blue) and ICMEs (orange) are shown.

Callaghan (2017) investigated cases of TCs, in which asymmetric inner core convection led to intensification. In the case of hurricane Hermine (2016) the storm rapidly transformed from a storm with a band of convection along its eastern side to a circular hurricane in around nine hours (Callaghan, 2017; their Section 6). Hurricane Hermine formed and intensified following arrivals of HSS/CIRs on August 30 and September 1 from two coronal holes (Fig. 7a). The intensification started with deep convection developing on the eastern side of the hurricane where the IR images showed cold cloud tops and "there was no strong indication of intensification at that time" (Callaghan, 2017; their Figure 20). This is further discussed in the next section.

Numerous studies by Callaghan (2024; and references therein) of strong asymmetric convection leading to rapid intensification of tropical cyclones investigated the role of a certain wind structures producing the vortical hot towers. "We have shown how winds turning anticyclonic from the 850 hPa level up to the 500 hPa level are associated with tropical

https://doi.org/10.5194/egusphere-2026-2327
Preprint. Discussion started: 1 June 2026

cyclone intensification" (Callaghan, 2024). The author called this wind structure Warm Air Advection (WAA) and listed their published studies, which include hurricanes, typhoons and southern hemisphere cyclones. We use this list of TCs in the SPE analysis of solar wind parameters keyed to the first maximum of RI of 20+ kt/24 h (Fig. 8). This result is very similar to cases of TCs with CBs (Fig. 6) and indicates that the WAA cases of TCs tend to intensify following HSS/CIRs.

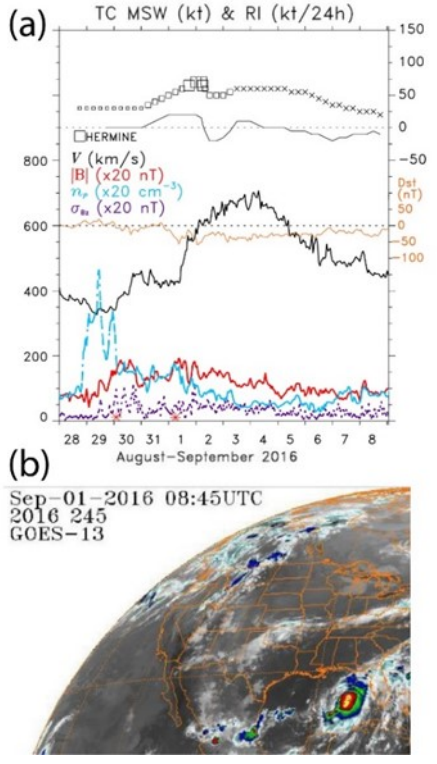

Figure 7: (a) The hourly OMNI solar wind data of V (green), B (red), n_p (broken light blue) and σ_{Bz} (dotted purple) are shown with the left y-axis scale factors printed. The geomagnetic storm index Dst is shown (orange line). Red asterisks on the time axis indicate CIRs. At the top, the "best track" data of hurricane Hermine. **(b)** The GOES-13 infrared image in September 2016 (https://www.ncdc.noaa.gov/gibbs/).

https://doi.org/10.5194/egusphere-2026-2327
Preprint. Discussion started: 1 June 2026

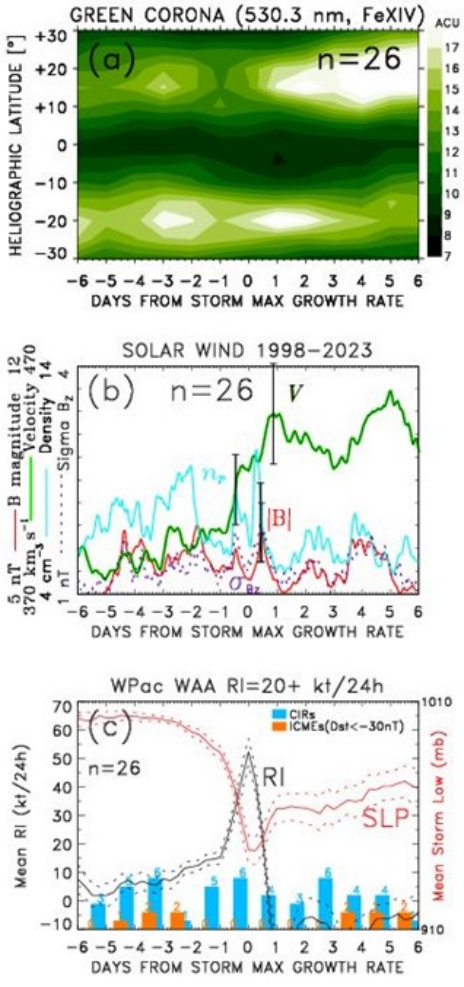

Figure 8: The same as Fig. 6 but for TCs that were identified as WAA events by Callaghan (2024).

Price et al. (2009) suggested that increased lightning activity in tropical cyclones are related to enhanced convection, which in turn leads to the intensification of TCs. They investigated the evolution of maximum winds and total lightning frequency during the lifetime of 56 TCs around the globe from 2005 to 2007 and found that in all cases, “lightning frequency and maximum sustained winds are significantly correlated (mean correlation coefficient of 0.82), where the maximum sustained winds and minimum pressures in hurricanes (sic) are preceded by increases in lightning activity approximately one day before the peak winds” (Price et al., 2009). We used these cases of TCs that included hurricanes, typhoons and cyclones in the SPE analysis of solar wind parameters keyed to the first maximum of RI of 30+ kt/24 h. The results that can be viewed in the Supplement Figure S4 reveal similar patterns discussed in Figs. 6 and 8 thus further supporting the conclusions that RIs of TCs with CB episodes show a tendency to follow arrivals of HSS/CIRs.

https://doi.org/10.5194/egusphere-2026-2327
Preprint. Discussion started: 1 June 2026

6 Assessment of CSI and slantwise convection in tropical cyclones

Prikryl et al. (2009b) and Prikryl (2024) suggested that down-going aurorally generated AGWs that can over-reflect in the warm frontal zone of extratropical cyclones contribute to CSI release, resulting in slantwise convection, series of cloud/rain bands and intensification of the storm.

In tropical cyclones, Möller and Shapiro (2002) and Bui et al. (2009) found small regions of symmetric instability in the mature tropical cyclone outflow layer. Molinari et al. (2012) calculated convective available potential energy (CAPE) and the vertical distribution of buoyancy using many dropsonde soundings collected by an aircraft. Although "upright buoyancy is less than slantwise buoyancy owing to upper-tropospheric warming in the storm core", slantwise convection could not be calculated in their study (Molinari et al., 2012). In a similar dropsonde study of a major hurricane Ivan (2004) conditions for both dry and moist symmetric instability were observed over a wider region than inertial instability (Molinari and Vollaro, 2014).

Chen et al. (2018) assessed CSI and slantwise convection in frontal zones of extratropical cyclones using ERA-Interim reanalysis data. We use this method with the ERA5 reanalysis to investigate the presence of CSI and likelihood of slantwise convection in the cases of tropical cyclones. SCAPE, SCAPE-CAPE residual, and vertically integrated extent of realizable symmetric instability (VRS) (e.g., Glinton et al., 2017; Chen et al., 2018) are calculated.

For the case of hurricane Hermine discussed in the previous section, Fig. 9a shows high SCAPE, with SCAPE sometimes exceeding CAPE (SCAPE-CAPE shown in red contours). This indicates convective available potential energy for a slantwise ascending air parcel from the low levels. Although, unlike the cases of frontal zones of extratropical cyclones (Chen et al., 2018; Prikryl, 2024), CAPE and SCAPE values are similar in tropical cyclones, both upright and slantwise buoyancy is possible. Fig. 9b shows 1-h accumulated precipitation, and in Figure 9c, VRS shows the thickness of air layer (measured in pressure) where conditional symmetric instability (CSI), high relative humidity, and vertical motion coexist (Chen et al., 2018).

In Fig. 9d, high vertical wind shear combined with strong low-level southerly winds are favorable conditions for over-reflection of down-going AGWs encountering opposing wind and vertical wind shears, and may be amplified (Prikryl and Rušin, 2023; their Section 6). The AGWs could have contributed to the release of CSI leading to the band of convection along the eastern side of hurricane Hermine.

https://doi.org/10.5194/egusphere-2026-2327
Preprint. Discussion started: 1 June 2026

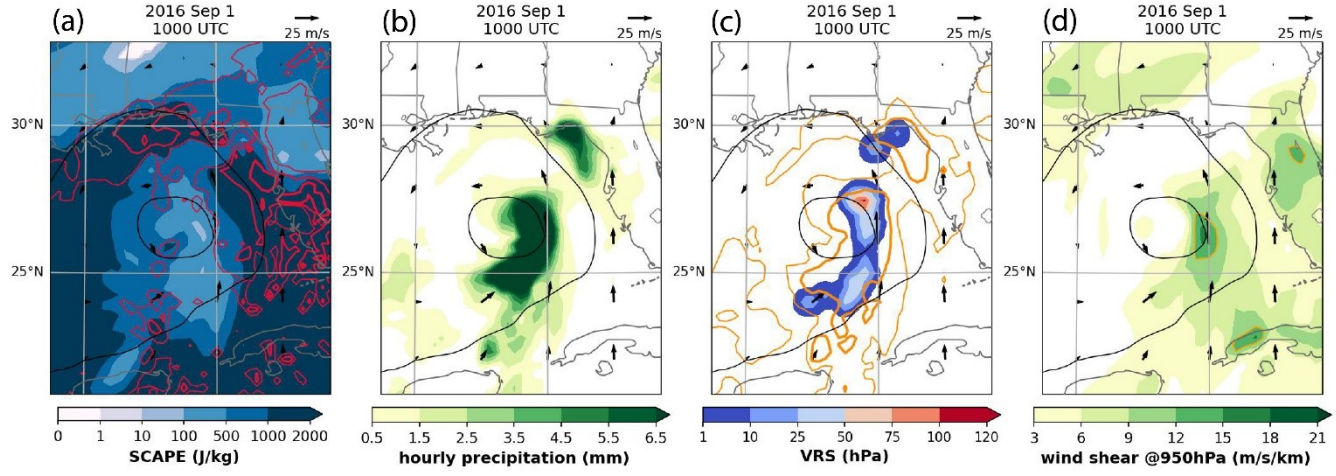

Figure 9: **(a)** SCAPE (shaded), SCAPE-CAPE (red contours; 100, 300, 500 J/kg), **(b)** 1-h accumulated precipitation (shaded), **(c)** VRS (shaded), precipitation (yellow contours; 0.5, 5.5 mm/h), **(d)** low-level wind shear (yellow contour; 12, 18 m/s/km). In all panels, the wind vectors (m/s) and the geopotential height (black contours at intervals of 50 m) at 950 hPa, are shown.

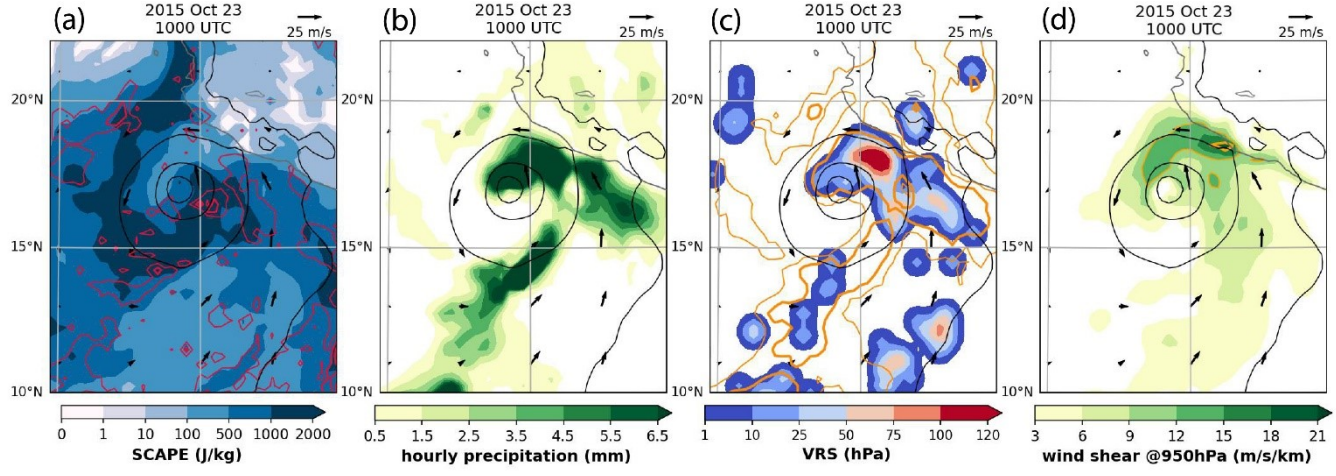

Figure 10: The same as Fig. 9 but for hurricane Patricia.

Similar argument can be made in the case of hurricane Patricia (one of the WAA cases; Callaghan, 2017) during the time of the major RI. Hurricane Patricia reached the maximum intensity at 1200 UT on October 23 (Fig. 4a). In Fig. 10, the ERA5 reanalysis at 1000 UT shows high SCAPE, VRS, as well as low-level vertical wind shear and low-level southerly winds along the eastern side of the hurricane Patricia. Similar results for typhoon Mangkhut and hurricane Ian can be viewed in the Supplement Figure S5.

https://doi.org/10.5194/egusphere-2026-2327
Preprint. Discussion started: 1 June 2026

In summary, the evaluation of SCAPE, SCAPE-CAPE residuals, and vertically integrated extent of realizable symmetric instability along with low-level wind and vertical wind shears in cases of tropical cyclones support the proposed mechanism that over-reflecting aurorally generated gravity waves could contribute to the release of CSI leading to slantwise convection and intensification of TCs.

7 AGWs generated in the lower thermosphere at high latitudes

As suggested by Prikryl et al. (2009b) and further discussed by Prikryl et al. (2025; and references therein), solar wind coupling to magnetosphere-ionosphere-atmosphere modulates ionospheric currents at high latitudes, which are a source of AGWs that propagate globally from auroral sources in the lower thermosphere both upward and downward. They can reach the troposphere with attenuated amplitudes and contribute to CSI release (Prikryl, 2024).

Prikryl et al. (2019) suggested that the aurorally generated AGWs that are ducted in the lower atmosphere to low latitudes (Mayr at al., 2013) can play a role in triggering convective bursts in tropical cyclones. Using a ray tracing method in a model atmosphere (Prikryl et al., 2005) in cases of tropical cyclones, Prikryl et al. (2019) showed that AGWs from high-latitude sources at altitudes of ~110km ducted to low latitudes can reach troposphere. These AGWs, subject to amplification upon over-reflection, could interact with the tropical cyclone vortex when encountering strong wind in the vortex and contribute to CSI release as discussed in Section 6.

7.1 Ray tracing of AGWs prior to intensification of hurricane Ian in September 2022

In the case of hurricane Ian, we consider a possible source of AGWs launched by quasiperiodic intensifications of ionospheric currents observed by a magnetometer in Qaanaaq (Thule), Greenland. Figure 11 shows time series of the X component of ground magnetic field perturbations and the normalized FFT power spectrum of the detrended time series indicating a peak at a period of ~40 min. Similar to cases of raytracing of AGWs using the MSIS90 model atmosphere discussed by Prikryl et al. (2018; their Figure 15), Fig. 12 shows possible group paths of AGWs with a period of 40 min from a source at 110 km altitude including a ducted wave in the lower atmosphere reaching the troposphere beyond 4000 km in about 5.4 hours. Hypothetically, such AGWs could have contributed to the release of CIS and slantwise convection in the case of hurricane Ian as discussed in Section 6.

https://doi.org/10.5194/egusphere-2026-2327
Preprint. Discussion started: 1 June 2026

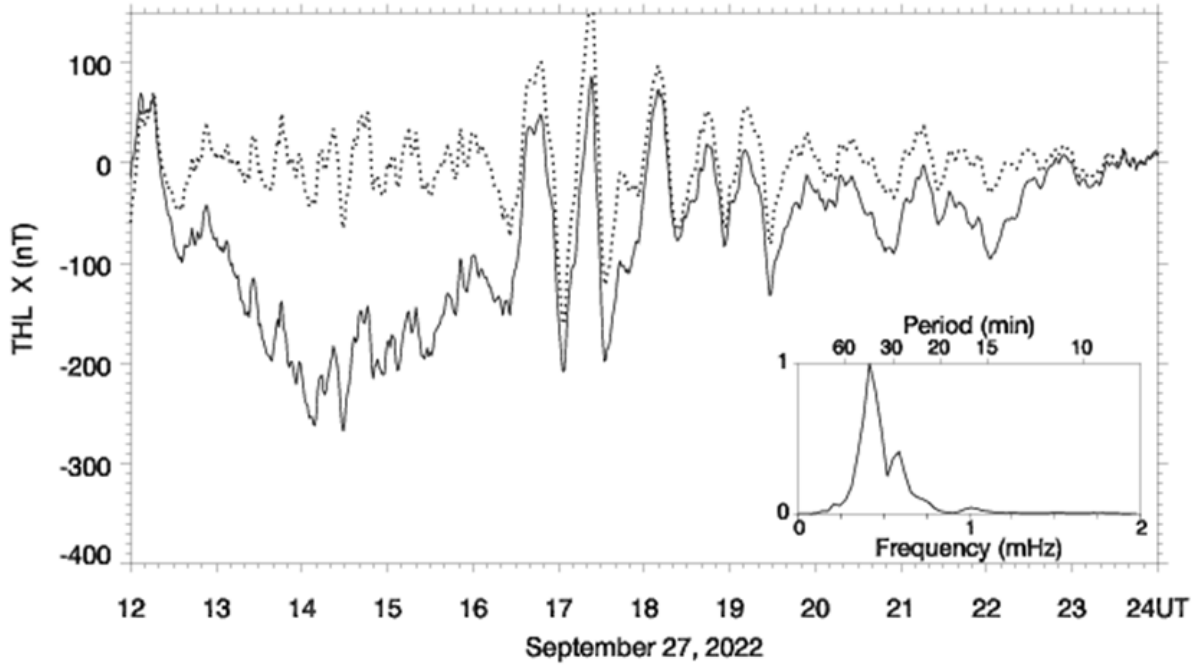

Figure 11: The X component of the ground magnetic field and the FFT power spectrum of the detrended time series (dotted line) observed by magnetometer in Qaanaaq (Thule), Greenland.

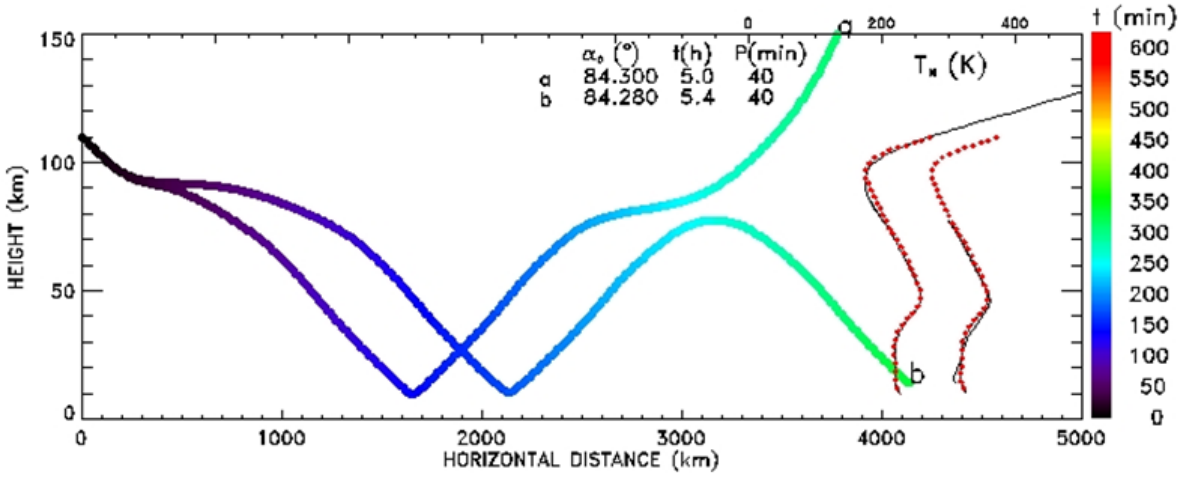

Figure 12: Ray paths for gravity waves with period 40 min launched from from a source at 110 km altitude in the MSIS90 model atmosphere. The rays are colour-coded by group time t. The neutral temperature $T_N(z)$ profiles for each ray are superposed. T_N for the first down leg path is shown in red dotted line. An offset of 100 °K is applied to the profiles for the ray b. Initial values α_0 of the wave vector $\boldsymbol{k}$ directions from horizontal, wave period P and group time t, are printed.

https://doi.org/10.5194/egusphere-2026-2327
Preprint. Discussion started: 1 June 2026

8 Mediterranean tropical-like cyclones

Emanuel (2005) who introduced the term "Mediterranean hurricane" that has since been abbreviated to "medicane", a Mediterranean Tropical-Like Cyclones (TLCs), showed that "standard baroclinic processes need not be called on to explain the final development, though they are probably necessary in the early stages" of TLC development. Most recently, Miglietta et al. (2025) proposed a definition of a medicane: "A medicane is a mesoscale cyclone that develops over the Mediterranean Sea and displays tropical-like cyclone characteristics: a warm core extending into the upper troposphere, an eye-like feature in its center with spiral cloud bands around, an almost windless center surrounded by nearly-symmetric sea surface wind circulation with maximum wind speed within a few tens of km from the center."

Davis and Bosart (2003) investigated baroclinically induced tropical cyclogenesis in the transition of subtropical cyclones into late season tropical storms and hurricanes during the 2000 and 2001 Atlantic tropical cyclone seasons. All transitioning cases initially started with the wind shear near, or more than, the upper limit of vertical shear deemed suitable for tropical cyclogenesis. In all cases, the shear eventually decreased during, or just prior to, the transition to tropical storms. Medicanes can also have a well-defined baroclinic precursor or remnant baroclinic structure. As Mazza et al. (2017) pointed out: "There is increasing evidence that the genesis of several medicanes or tropical-like cyclones in the Mediterranean basin can be interpreted as the result of the tropical transition of originally baroclinic cyclones (McTaggart-Cowan et al. 2010a,b; Chaboureau et al. 2012; Cioni et al. 2016)".

In Sections 3-5 we used the SPE analysis of solar wind variables to show that rapid intensification of tropical cyclones tends to follow arrivals of HSS/CIRs from coronal holes and/or impacts of ICMEs. We now use the SPE method in cases of medicanes compiled from published sources (Section 2). Figure 13 shows the SPE analysis of green corona intensity and the solar wind variables keyed to start dates of medicane storms. The mean green corona intensity depletions in Figure 13a are due to superposed coronal holes. Solar wind HSSs originating from these coronal holes are then superposed in Figure 13b that shows the mean solar wind velocity increasing from a minimum to a maximum after the key time. The mean solar wind density, the magnetic field and the standard deviation σ_{Bz} all peak just before the key time, which is mostly due to superposition of CIRs at the leading edge of HSSs from coronal holes. This pattern suggests that medicanes tend to develop following arrivals of HSSs.

https://doi.org/10.5194/egusphere-2026-2327
Preprint. Discussion started: 1 June 2026

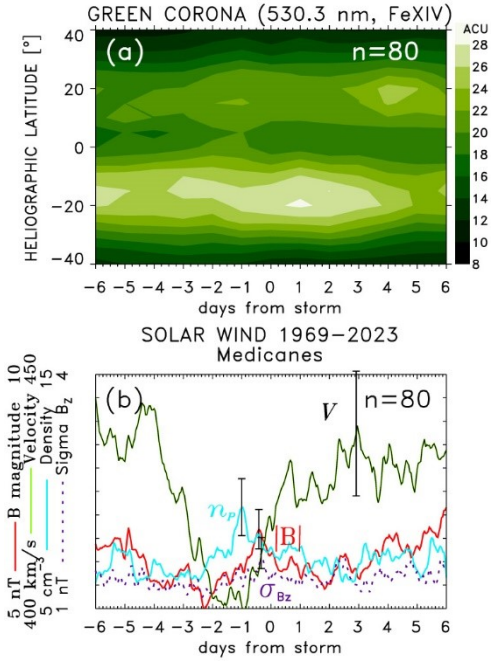

365 **Fig. 13.** The SPE analysis of **(a)** green corona intensity and **(b)** solar wind plasma parameters keyed to starting dates of medicane storm events.

To show this another way, Fig. 14a shows the SPE analysis of solar wind variables keyed to arrivals of HSS/CIRs that were associated with medicane storms. The results support the conclusion that most medicanes developed following arrivals of
370 HSS/CIRs. The bottom panel shows the histograms of the number of such storms. On the other hand, eight medicanes developed following impacts of ICMEs, as shown in Fig. 14b. Start dates of few medicane storms were associated with high-density plasma ahead of HCSs that typically closely precede HSS/CIRs. The rest of medicanes from the list used in Fig. 13 could not be associated with any specific solar wind disturbances, mostly because of data gaps.

https://doi.org/10.5194/egusphere-2026-2327
Preprint. Discussion started: 1 June 2026

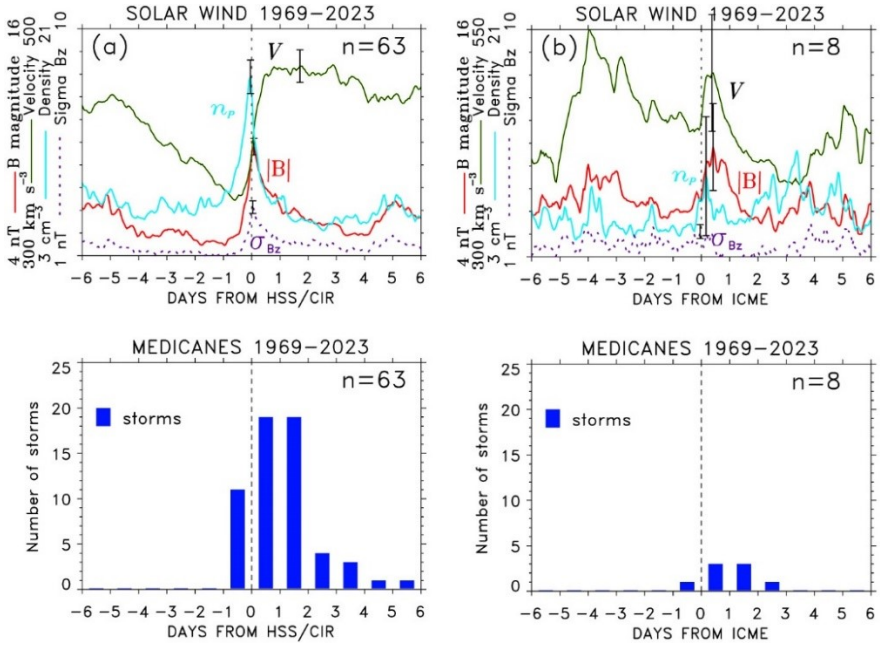

Fig. 14. The SPE analysis of solar wind plasma parameters keyed to **(a)** arrivals of HSS/CIRs and **(b)** impacts of ICMEs that were associated with starting dates of medicane storm events shown in the histograms in the bottom panels.

8.1 Cases of tropical-like cyclones in the context of solar wind

For cases of medicanes discussed in this section, Fig. 15 shows the hourly OMNI solar wind data (V, |B|, n_p, and σ_{Bz}) along with the geomagnetic storm index *Dst*. The red asterisks on the time axis indicate arrivals of HSS/CIRs. The minimum sea level pressure (MSLP) and the maximum wind speed at altitude of 10 m in the area ±5° latitude/longitude from the center of the storm are derived from the ERA5 reanalysis dataset are shown at the top of each panel. The Meteosat IR images of subtropical cyclones that developed into TLCs are shown at the bottom of Fig 15.

Reale and Atlas (2001) analyzed two anomalous Mediterranean cyclones that transitioned into TLCs between 3 and 10 October 1996. Both Samir (4–6 October) and Cornelia (7–9 October) developed following HSS/CIR arrivals (Figure 15a) from precursors baroclinic waves that crossed the Alps.

Pytharoulis (2018) studied an intense Mediterranean tropical-like cyclone Qendresa (7-9 November 2014), which formed south of Sicily from a low-pressure system that emerged from northern Libya on November 6, interacting with the front and transitioned into a TLC following arrival of a moderate HSS/CIR (Fig. 15b).

Medicane Lucia (13-14 April 2012) developed from a subtropical cyclone moving in the Mediterranean Sea from Atlantic while transitioning into tropical-like cyclone. The subtropical cyclone intensified as it developed a series of convective bands in the warm frontal zone following arrival of a strong HSS/CIR (above) that triggered a geomagnetic storm on April 12. This was very similar to cases of extratropical cyclones discussed by Prikryl (2024; their Figures 3 and 4).

https://doi.org/10.5194/egusphere-2026-2327
Preprint. Discussion started: 1 June 2026

In the next subsection, we use the ERA5 reanalysis to assess the presence of CSI and likelihood of slantwise convection in the transition of medicanes from their baroclinic precursors.

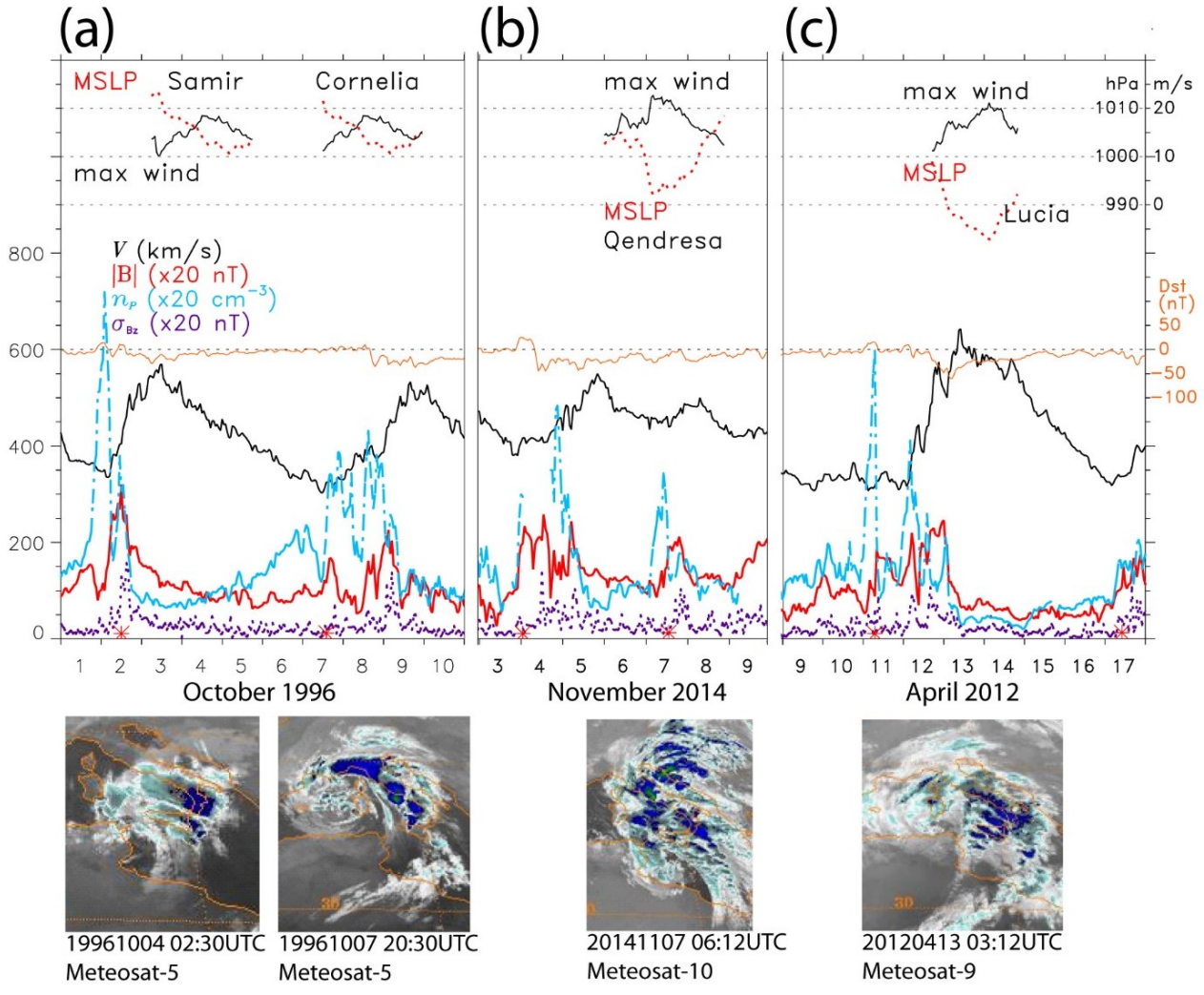

Figure 15. In the bottom half of each panel, the 1-hour OMNI solar wind data of V (green), **B** (red), n_p (broken light blue) and σ_{Bz} (dotted purple) are shown with the left y-axis scale factors printed. The geomagnetic storm index Dst is shown (orange line). Red asterisks on the time axis indicate arrivals of HSS/CIRs. In the top half of each panel, the ERA5 derived minimum MSLP and the maximum wind speed at 10 m in the area ±5° latitude/longitude from the center of the storm **(a)** Samir and Cornelia, **(b)** Qendresa, and **(c)** Lucia. The Meteosat IR images of subtropical cyclones that developed into TLCs are shown at the bottom.

https://doi.org/10.5194/egusphere-2026-2327
Preprint. Discussion started: 1 June 2026

8.2 Assessment of CSI and slantwise convection in the baroclinic precursors of medicanes

The Mediterranean subtropical cyclones that are baroclinic precursors of medicanes are subject to development similar to extratropical cyclones leading to their intensification and potential transition to tropical-like cyclones. Using ERA5 reanalysis (Prikryl, 2024) the presence of CSI and likelihood of slantwise convection can be assessed in the cases of tropical-like cyclones that transitioned from intensifying subtropical cyclones. For storms Samir, Cornelia, Qendresa, and Lucia before their transition to TCLs, Fig. 16a shows high SCAPE, with SCAPE exceeding CAPE (SCAPE-CAPE shown in red contours) in the frontal zones of their baroclinic precursors. This indicates convective available potential energy for a slantwise ascending air parcel from the low levels. Fig. 16b shows 1-h accumulated precipitation with red contours showing the fractional SCAPE residual f_s = (SCAPE-CAPE)/SCAPE. A closer-to-one f_s indicates the relative dominance of slantwise over upright convection. In Fig. 16c, VRS shows the thickness of air layer (measured in pressure) where conditional symmetric instability (CSI), high relative humidity, and vertical motion coexist (Chen et al., 2018). In Fig. 16d, vertical wind shear combined with low-level southerly winds are the conditions conducive to over-reflection of down-going AGWs encountering opposing wind and vertical wind shears (Prikryl and Rušin, 2023; 2025) that can potentially contribute to CSI release, slantwise convection, cloud bands and high-rate precipitation.

It is found that the highest values of SCAPE, f_S and VRS are associated with noteworthy features of the intensifying cyclones. In the case of Qendresa, a baroclinic leaf, a comma head and the cloud hook (https://user.eumetsat.int/resources/case-studies/mediterranean-cyclones-medicanes-2007-2021#ID-Qendresa-7-8-Nov). As it extends in length with time, the baroclinic leaf is structured by a series of rain bands, series of convection cells, resulting in "back building" mesoscale convective lines (Bluestein and Jain, 1985). This is in the region where CSI exists, and the slantwise convection can be initiated by incoming equatorward propagating AGWs even though their amplitudes are significantly attenuated. In the case Lucia, a striated delta cloud (Fig. 15c) is co-located with low-level southerly winds and wind shears evaluated between 900 and 1000hPa levels (Fig. 16d) - the conditions favourable for over-reflection of equatorward propagating down-going AGWs. It has been shown that such features, including comma heads and striated delta clouds, which often characterize rapidly intensifying extratropical cyclones, tend to occur following arrivals HSS/CIRs when large amplitude of AGWs are generated at high latitudes ((Prikryl and Rušin, 2023).

Other cases of medicanes Rolf, Ruven (also known as Cleopatra), Isabela, and Trudy and their baroclinic precursors in the context of solar wind are shown in the Supplement Figures S6 and S7.

https://doi.org/10.5194/egusphere-2026-2327
Preprint. Discussion started: 1 June 2026

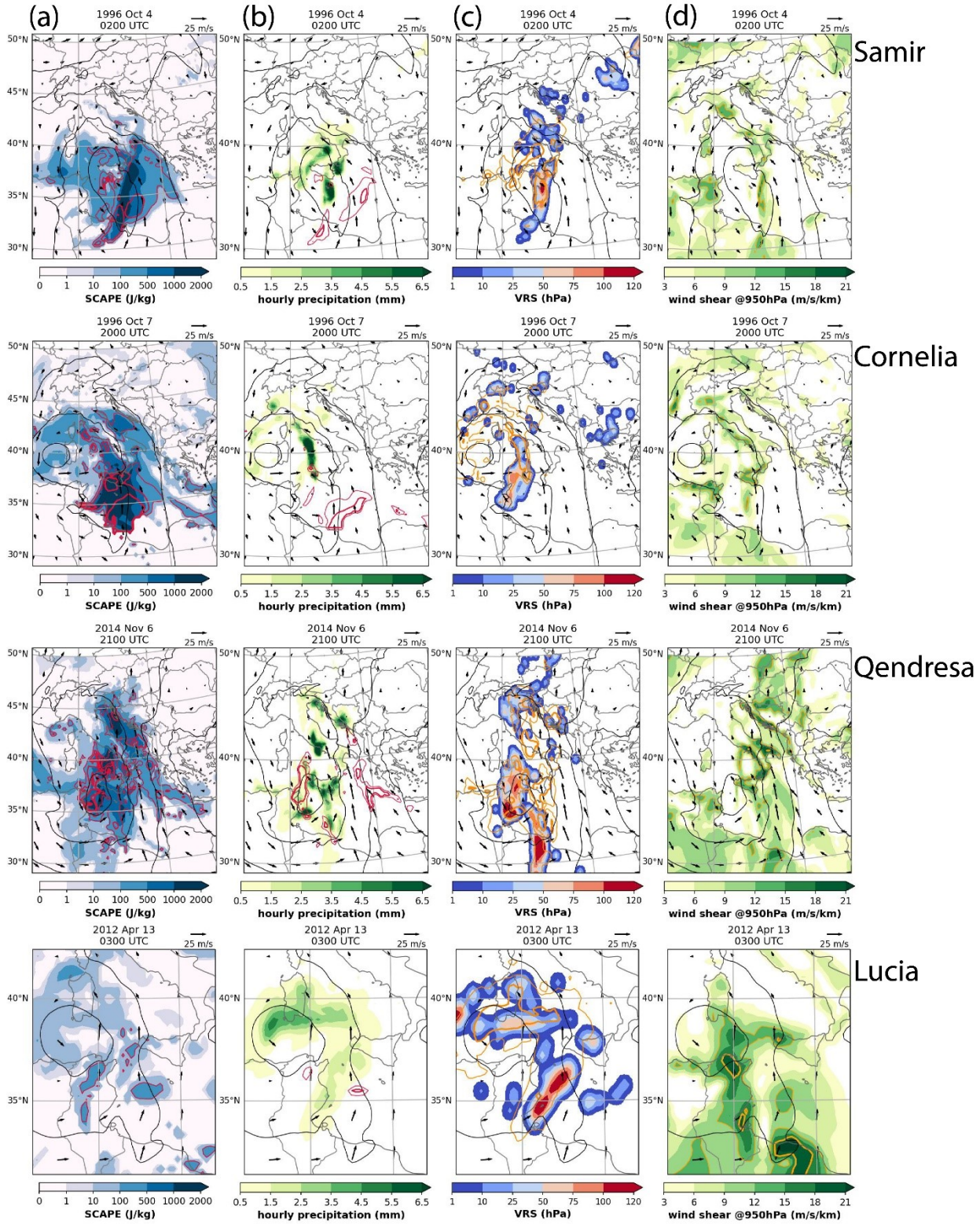

https://doi.org/10.5194/egusphere-2026-2327
Preprint. Discussion started: 1 June 2026

Figure 16. (a) SCAPE (shaded), SCAPE-CAPE (red contours; 100, 300, 500 J/kg), **(b)** 1-h accumulated precipitation (shaded) and f_s (red contours; thin for 0.5 and thick for 0.8), **(c)** VRS (shaded), precipitation (yellow contours; 0.5, 5.5 mm/h), **(d)** low-level wind shear (yellow contour; 12, 18 m/s/km). In all panels, the wind vectors (m/s) and the geopotential height (black contours at intervals of 50 m) at 950 hPa are shown.

9 Summary and Conclusions

Using the superposed epoch analysis method, it is found that rapid intensification of a large percentage of tropical cyclones follow arrivals of solar wind high-speed streams from coronal holes and impacts of interplanetary coronal mass ejections. Similarly, the superposed epoch analysis of solar wind variables keyed to start dates of medicane storms indicates that Mediterranean tropical-like cyclones tend to develop from their baroclinic precursors following arrivals of HSSs or ICMEs. It is suggested that aurorally generated atmospheric gravity waves can contribute to the development of tropical cyclones and Mediterranean tropical-like cyclones. While these gravity waves reach the troposphere with attenuated amplitudes, they can contribute to the release of conditional symmetric instability. We use the ERA5 meteorological re-analysis to evaluate slantwise convective available potential energy (SCAPE) and show cases of tropical cyclones and Mediterranean tropical-like cyclones displaying high values of SCAPE, SCAPE-CAPE residuals, and vertically integrated extent of realizable symmetric instability that can be released by over-reflecting aurorally generated gravity waves encountering low-level opposing wind and vertical wind shears leading to slantwise convection and intensification of the storms.

Data availability

The revised HURDAT2 database (http://www.nhc.noaa.gov/data/) of “best tracks” of tropical and subtropical cyclones for the Atlantic and East Pacific basins is provided by the National Hurricane Center (NHC). The U.S. government website Joint Typhoon Warning Center (JTWC) is hosted by several agencies including National Oceanic and Atmospheric Administration (NOAA) and National Weather Service (NWS). The products and services include the Tropical Cyclone Best Track Data http://www.metoc.navy.mil/jtwc/jtwc.html?best-tracks that cover Southern Hemisphere, Northern Indian Ocean and Western North Pacific Ocean. The ERA5 reanalysis dataset is available at https://doi.org/10.24381/cds.bd0915c6 (Hersbach et al., 2020, 2023). The National Space Science Data Center (NSSDC) OMNIWeb at http://omniweb.gsfc.nasa.gov provides the solar wind data (King and Papitashvili, 2005). The Modified Homogeneous Data Set of Coronal Intensities (Dorotovič et al., 2014) is accessible at https://www.kozmos-online.sk/slnko/modifikovany-homogenny-rad-modified-homogeneous-data-set/ (KOZMOS, 2025).

Supplement

The supplement related to this article will be available online.

https://doi.org/10.5194/egusphere-2026-2327
Preprint. Discussion started: 1 June 2026

Author contributions

PP: conceptualization, formal analysis, investigation, methodology, project administration, resources, software, supervision, validation, visualization, writing original draft, review, and editing. VR: conceptualization, formal analysis of coronal data, investigation, methodology, resources, validation, review, and editing.

Competing interests

The contact author has declared that neither of the authors has any competing interests.

Disclaimer

Copernicus Publications remains neutral with regard to jurisdictional claims made in the text, published maps, institutional affiliations, or any other geographical representation in this paper. While Copernicus Publications makes every effort to include appropriate place names, the final responsibility lies with the authors.

Acknowledgements

This research was supported by the University of New Brunswick and by the VEGA project 2/0043/24 (Slovak Academy of Sciences). The authors would like to thank Ting-Chen Chen at the Institute of Meteorology and Climate Research, Karlsruhe Institute of Technology, for sharing the computer code for the analysis of conditional symmetric instability. The reanalysis dataset ERA5 is a product of the European Centre for Medium-Range Weather Forecasts (ECMWF). We acknowledge contributions by the NOAA National Hurricane Center and the Hurricane Research Division of AOML, and the Joint Typhoon Warning Center providing public-free access to data sets. Contributions by the ACE, Geotail, IMP-8, SoHO and Wind spacecraft teams, the NSSDC OMNIWeb and SuperDARN are acknowledged. SuperDARN is a collection of radars funded by many national scientific funding agencies around the world. The ground magnetometer data used in this paper were collected at magnetic observatories. We thank the national institutes that support them and INTERMAGNET for promoting high standards of magnetic observatory practice (www.intermagnet.org). We are grateful to many institutions for providing access to meteorological data, including the Cooperative Institute for Meteorological Satellite Studies, University of Wisconsin-Madison (CIMSS) Tropical Cyclone Team, Environment Canada, Japan Meteorological Agency, Australian Government Bureau of Meteorology and Engineering Center and the University of Washington, Department of Atmospheric Sciences.

Financial support

Vojto Rušin is supported by the VEGA project 2/0043/24 (Slovak Academy of Sciences).

https://doi.org/10.5194/egusphere-2026-2327
Preprint. Discussion started: 1 June 2026

Review statement

The review statement will be added by Copernicus Publications listing the handling editor as well as all contributing referees according to their status anonymous or identified.

References

Ambrož, P.: Statistical method of superposition of epochs. I-Methodical analysis and some criteria of application, Bull. Astron. Inst. Czechoslov., 30, 114–121, 1979.

Avenas, A., Marcello Miglietta, M., Mouche, A., Dafis, S., Colin, A., Husson, R., and Flaounas, E.: Medicane characteristics from high-resolution satellite radar observations. Quart. J. Roy. Meteor. Soc., e70102, https://doi.org/10.1002/qj.70102, 2026.

Bluestein, H. B. and Jain, M. H.: Formation of mesoscale lines of precipitation: Severe squall lines in Oklahoma during the spring, J. Atmos. Sci., 42, 1711–1732, https://doi.org/10.1175/1520-0469(1985)042<1711:FOMLOP>2.0.CO;2, 1985.

Borzì, A. M., Cannata, A., Panzera, F., D'Amico, S., Lo Re, C., and Aster, R. C.: Microseism amplitude and wave power in the Mediterranean Sea (1996–2023). Journal of Geophysical Research: Solid Earth, 130, e2024JB030528. https://doi.org/10.1029/2024JB030528, 2025.

Bosart, L. F., and Bartlo, J. A.: Tropical Storm Formation in a Baroclinic Environment. Mon. Wea. Rev., 119, 1979–2013, https://doi.org/10.1175/1520-0493(1991)119<1979:TSFIAB>2.0.CO;2, 1991.

Bui, H. H., R. K. Smith, M. T. Montgomery, and J. Peng, 2009: Balanced and unbalanced aspects of tropical-cyclone intensification. Quart. J. Roy. Meteor. Soc., 135, 1715–1731, doi:10.1002/qj.502.

Burlaga, L., Sittler, E., Mariani, F., and Schwenn, R.: Magnetic loop behind an interplanetary shock: Voyager, Helios, and IMP 8 observations, J. Geophys. Res., 86, 6673–6684, https://doi.org/10.1029/JA086iA08p06673, 1981.

Callaghan, J.: Asymmetric inner core convection leading to tropical cyclone intensification, Trop. Cyclone Res. Rev., 6(3-4), 55-66, 10.6057/2017TCRRh3.02, 2017.

Callaghan, J.: Development of strong asymmetric convection leading to rapid intensification of tropical cyclones, Trop. Cyclone Res. Rev., 13(4), 239-260, https://doi.org/10.1016/j.tcrr.2024.11.006, 2024.

Chaboureau, J.-P., Pantillon, F., Lambert, D., Richard, E., and Claud, C.: Tropical transition of a Mediterranean storm by jet crossing. *Quart. J. Roy. Meteor. Soc.*, ***138***, 596–611, doi:10.1002/qj.960, 2012.

Chen, H., and Zhang, D.: On the Rapid Intensification of Hurricane Wilma (2005). Part II: Convective Bursts and the Upper-Level Warm Core. J. Atmos. Sci., 70, 146–162, https://doi.org/10.1175/JAS-D-12-062.1, 2013.

Chimonas, G. and Hines, C. O.: Atmospheric gravity waves launched by auroral currents, Planet. Space Sci., 18, 565–582, https://doi.org/10.1016/0032-0633(70)90132-7, 1970.

Cioni, G., Malguzzi, P., and Buzzi, A.: Thermal structure and dynamical precursor of a Mediterranean tropical-like cyclone. *Quart. J. Roy. Meteor. Soc.*, ***142***, 1757–1766, doi:10.1002/qj.2773, 2016.

https://doi.org/10.5194/egusphere-2026-2327
Preprint. Discussion started: 1 June 2026

Dafis S, Claud C, Kotroni V, Lagouvardos K, Rysman J-F.: Insights into the convective evolution of Mediterranean tropical-like cyclones. Q J R Meteorol Soc. 146: 4147–4169. https://doi-org.proxy.hil.unb.ca/10.1002/qj.3896, 2020.

Davis, C. A., and L. F. Bosart, 2003: Baroclinically Induced Tropical Cyclogenesis. *Mon. Wea. Rev.*, **131**, 2730–2747, https://doi.org/10.1175/1520-0493(2003)131<2730:BITC>2.0.CO;2.

Diakakis, M., Mavroulis, S., Filis, C., Lozios, S., Vassilakis, E., Naoum, G., Soukis, K., Konsolaki, A., Kotsi, E., Theodorakatou, D., et al. Impacts of Medicanes on Geomorphology and Infrastructure in the Eastern Mediterranean, the Case of Medicane Ianos and the Ionian Islands in Western Greece. Water 15, 1026. https:// doi.org/10.3390/w15061026, 2023.

DeMaria, M., Sampson, C.R., Knaff, J.A., and Musgrave, K.D.: Is tropical cyclone intensity guidance improving? Bull. Amer. Meteor. Soc., 95, 387–398, https://doi.org/10.1175/BAMS-D-12-00240.1, 2014.

DeMaria, M., Franklin, J.L., Onderlinde, M.J., and Kaplan, J.: Operational forecasting of tropical cyclone rapid intensification at the national hurricane center. Atmosphere, 12, 683, https://doi.org/10.3390/atmos12060683, 2021.

Dungey, J. W.: Interplanetary Magnetic Field and the Auroral Zones, Phys. Rev. Lett. 6, 47–48, https://doi.org/10.1103/PhysRevLett.6.47, 1961.

Dungey, J. W.: Origin of the concept of reconnection and its application to the magnetopause: A historical view, Physics of the Magnetopause, in: Geophysical Monograph 90, edited by: Song, P., Sonnerup, B. U. O., and Thomsen, M. F., AGU, Washington, D.C., 17–19, https://doi.org/10.1029/GM090p0017, 1995.

Emanuel, K.: Genesis and maintenance of "Mediterranean hurricanes", Adv. Geosci., 2, 217–220, https://doi.org/10.5194/adgeo-2-217-2005, 2005.

Glinton, M., Gray, S. L., Chagnon, J. M., and Morcrette, C. J.: Modulation of precipitation by conditional symmetric instability release. Atmos. Res., 185, 186–201, https://doi.org/10.1016/j.atmosres.2016.10.013, 2017.

Gonzalez, W. D., Joselyn, J. A., Kamide, Y., Kroehl, H. W., Rostoker, G., Tsurutani, B. T., et al.: What is a geomagnetic storm? J. Geophys. Res. Space Phys. 99 (A4), 5771–5792. doi:10.1029/93ja02867, 1994.

Gopalswamy, N.: History and development of coronal mass ejections as a key player in solar terrestrial relationship, Geosci. Lett., 3, 8, https://doi.org/10.1186/s40562-016-0039-2, 2016.

Guimond, S. R., G. M. Heymsfield, and F. J. Turk, 2010: Multiscale observations of Hurricane Dennis (2005): The effects of hot towers on rapid intensification. J. Atmos. Sci., 67, 633–654.

Hendricks, E. A.: Internal Dynamical Control on Tropical Cyclone Intensity Variability – A Review. Tropical Cyclone Research and Review, 1(1), 97-105, https://doi.org/10.6057/2012TCRR01.11. 2012.

Hendricks, E. A., Montgomery, M. T., and Davis, C. A.: The Role of "Vortical" Hot Towers in the Formation of Tropical Cyclone Diana (1984). J. Atmos. Sci., 61, 1209–1232, https://doi.org/10.1175/1520-0469(2004)061<1209:TROVHT>2.0.CO;2., 2004.

Hérincs, D., Dezső, Z.: Mikrohullámú tartományú műholdas mérések használata medikánok esetén (Use of microwave satellite measurements in case of medicanes). Légkör, 69(3), 171-171. DOI:10.56474/legkor.2024.3.2, 2024.

https://doi.org/10.5194/egusphere-2026-2327
Preprint. Discussion started: 1 June 2026

Hines, C. O.: Motions of the neutral atmosphere, in: Physics of the Earth's Upper Atmosphere, edited by: Hines, C. O., Paghis, I., Hartz, T. R., and Fejer, J. A., Prentice-Hall, Inc., London, ISBN-10 0136722792, 1965.

Hocke, K. and Schlegel, K.: A review of atmospheric gravity waves and travelling ionospheric disturbances: 1982–1995, Ann. Geophys., 14, 917–940, https://doi.org/10.1007/s00585-996-0917-6, 1996.

Horinouchi, T., Yanase, T., Ohta, Y., Matsuoka, D., Kitamoto, A., Shimada, U., Yoshida, R., and Fudeyasu, H.: Statistical Prediction of Tropical Cyclone Rapid Intensification with Explainable AI. *Wea. Forecasting*, **40**, 1859–1875, https://doi.org/10.1175/WAF-D-24-0228.1, 2025.

Huang, L., Wan, Q. L., Liu C. X., et al.: Ensemble based diagnosis of the track errors of Super Typhoon Mangkhut (2018). J. Meteor. Res., 34(2), 353–367, doi: 10.1007/s13351-020-9086-x, 2020.

Kaplan, J., DeMaria M., and Knaff J. A.: A Revised Tropical Cyclone Rapid Intensification Index for the Atlantic and Eastern North Pacific Basins. *Wea. Forecasting*, **25**, 220–241, https://doi.org/10.1175/2009WAF2222280.1, 2010.

Knapp, K. R.: Scientific data stewardship of International Satellite Cloud Climatology Project B1 global geostationary observations. Journal of Applied Remote Sensing, 2, 023548, 2008, doi:10.1117/1.3043461

Krieger, A. S., Timothy, A. F., and Roelof, E. C.: A coronal hole and its identification as the source of a high velocity solar wind stream, Sol. Phys., 29, 505–525, https://doi.org/10.1007/BF00150828, 1973.

Landsea, C.W., Franklin, J.L.: Atlantic hurricane database uncertainty and pre sentation of a new database format. Mon. Weather Rev. 141, 3576–3592, 2013.

Li, X., Cheng, X., Fei, J., Huang, X., and He, S.: Evolution of the double warm-core structure in the eyewall replacement cycle of Typhoon Trami (2018). Journal of Geophysical Research: Atmospheres, 129, e2024JD041371. https://doi.org/10.1029/2024JD041371, 2024.

Marra, A. C., Federico, S., Montopoli, M., Avolio, E., Baldini, L., Casella, D., D'Adderio, L. P., Dietrich, S., Sanò, P., Torcasio, R. C., and Panegrossi, G.: The Precipitation Structure of the Mediterranean Tropical-Like Cyclone Numa: Analysis of GPM Observations and Numerical Weather Prediction Model Simulations. Remote Sensing, 11(14), 1690. https://doi.org/10.3390/rs11141690, 2019.

Mayr, H. G., Talaat, E. R., and Wolven, B. C.: Global propagation of gravity waves generated with the whole atmosphere transfer function model, J. Atmos. Sol.-Terr. Phy., 104, 7–17, https://doi.org/10.1016/j.jastp.2013.08.001, 2013.

McWilliams, K.A., Yeoman, T.K., and Cowley, S.W.H.: Two-dimensional electric field measurements in the ionospheric footprint of a flux transfer event, Ann. Geophys., 18, 1584–1598, 2001.

McTaggart-Cowan, R., Galarneau, T. J., Bosart, L. F., and Milbrandt, J. A.: Development and tropical transition of an Alpine lee cyclone. Part I: Case analysis and evaluation of numerical guidance. Mon. Wea. Rev., 138, 2281–2307, https://doi.org/10.1175/2009MWR3147.1, 2010a.

McTaggart-Cowan, R., Galarneau, T. J., Bosart, L. F., and Milbrandt, J. A.: Development and Tropical Transition of an Alpine Lee Cyclone. Part II: Orographic Influence on the Development Pathway. Mon. Wea. Rev., 138, 2308–2326, https://doi.org/10.1175/2009MWR3148.1, 2010b.

https://doi.org/10.5194/egusphere-2026-2327
Preprint. Discussion started: 1 June 2026

Miglietta, M. M., and Coauthors: Defining Medicanes: Bridging the Knowledge Gap between Tropical and Extratropical Cyclones in the Mediterranean. Bull. Amer. Meteor. Soc., 106, E1955–E1971, https://doi.org/10.1175/BAMS-D-24-0289.1, 2025.

Miglietta, M. M., Laviola, S., Malvaldi, A., Conte, D., Levizzani, V., and Price, C.: Analysis of tropical-like cyclones over the Mediterranean Sea through a combined modeling and satellite approach, Geophys. Res. Lett., 40, 2400–2405, doi:10.1002/grl.50432, 2013.

Miglietta, M.M., Mastrangelo, D., Conte, D.: Influence of physics parameterization schemes on the simulation of a tropical-like cyclone in the Mediterranean Sea. Atmos. Res. 153, 360–375. http://dx.doi.org/10.1016/j.atmosres.2014.09.008, 2015.

Miglietta, M.M., Cerrai, D., Laviola, S., Cattani, E., Levizzani, V.: Potential vorticity patterns in Mediterranean "hurricanes". Geophys. Res. Lett. http://dx.doi.org/10. 1002/2017GL072670, 2017.

Milan, S.E., Lester, M., Cowley, S.W.H., and Brittnacher, M.: Convection and auroral response to a southward turning of the IMF: Polar UVI, CUTLASS and IMAGE signatures of transient magnetic flux transfer at the magnetopause, J. Geophys. Res., 105, 15,741–15,755, 2000. doi:10.1029/2000JA900022.

Molinari, J., Romps, D. M., Vollaro, D., and Nguyen, L.: CAPE in Tropical Cyclones. J. Atmos. Sci., 69, 2452–2463, https://doi.org/10.1175/JAS-D-11-0254.1, 2012.

Molinari, J., and Vollaro, D.: Symmetric Instability in the Outflow Layer of a Major Hurricane. J. Atmos. Sci., 71, 3739–3746, https://doi.org/10.1175/JAS-D-14-0117.1, 2014.

Möller, J. D., and Shapiro, L. J.: Balanced Contributions to the Intensification of Hurricane Opal as Diagnosed from a GFDL Model Forecast. Mon. Wea. Rev., 130, 1866–1881, https://doi.org/10.1175/1520-0493(2002)130<1866:BCTTIO>2.0.CO;2, 2002.

Montgomery, M. T., Nicholls, M. E., Cram, T. A., and Saunders, A. B.: A Vortical Hot Tower Route to Tropical Cyclogenesis. J. Atmos. Sci., 63, 355–386, https://doi.org/10.1175/JAS3604.1, 2006.

P.T. Nastos, Papadimou, K.K., and Matsangouras, I.T.: Mediterranean tropical-like cyclones: impacts and composite daily means and anomalies of synoptic patterns, Atmos. Res., 208, pp. 156-166, 10.1016/j.atmosres.2017.10.023, 2018.

Price, C., Asfur, M., and Yair, Y.: Maximum hurricane intensity preceded by increase in lightning frequency. Nat. Geosci., 2, 329–332, 2009.

Prikryl, P.: Mesoscale weather influenced by auroral gravity waves contributing to conditional symmetric instability release?, Adv. Sci. Res., 21, 1–17, https://doi.org/10.5194/asr-21-1-2024, 2024.

Prikryl, P., Rušin, V., and Rybanský, M.: The influence of solar wind on extratropical cyclones – Part 1: Wilcox effect revisited, Ann. Geophys., 27, 1–30, https://doi.org/10.5194/angeo-27-1-2009, 2009a.

Prikryl, P., Muldrew, D. B., and Sofko, G. J.: The influence of solar wind on extratropical cyclones – Part 2: A link mediated by auroral atmospheric gravity waves?, Ann. Geophys., 27, 31–57, https://doi.org/10.5194/angeo-27-31-2009, 2009b.

https://doi.org/10.5194/egusphere-2026-2327
Preprint. Discussion started: 1 June 2026

Prikryl, P., Iwao, K., Muldrew, D. B., Rušin, V., Rybanský, M., and Bruntz, R.: A link between high-speed solar wind streams and explosive extratropical cyclones, J. Atmos. Sol.-Terr. Phy., 149, 219–231, https://doi.org/10.1016/j.jastp.2016.04.002, 2016.

Prikryl, P., Bruntz, R., Tsukijihara, T., Iwao, K., Muldrew, D. B., Rušin, V., Rybanský, M., Turňa, M., and Šťastný, P.: Tropospheric weather influenced by solar wind through atmospheric vertical coupling downward control, J. Atmos. Sol.-Terr. Phy., 171, 94–110, https://doi.org/10.1016/j.jastp.2017.07.023, 2018.

Prikryl, P., Nikitina, L., and Rušin, V.: Rapid intensification of tropical cyclones in the context of the solar wind-magnetosphere-ionosphere-atmosphere coupling, J. Atmos. Sol.-Terr. Phy., 183, 36–60, https://doi.org/10.1016/j.jastp.2018.12.009, 2019.

Prikryl P. and Rušin V.: Occurrence of heavy precipitation influenced by solar wind high-speed streams through vertical atmospheric coupling. Front. Astron. Space Sci. 10:1196231, doi: 10.3389/fspas.2023.1196231, 2023.

Prikryl P. and Rušin V.: Occurrence of Tornado Outbreaks Influenced by Solar Wind-Magnetosphere Ionosphere-Atmosphere Coupling, Adv. Sci. Res., 22, 19–38, https://doi.org/10.5194/asr-22-19-2025, 2025.

Pytharoulis, I., Kartsios, S., Tegoulias, I., Feidas, H., Miglietta, M. M., Matsangouras, I., and Karacostas, T.: Sensitivity of a Mediterranean Tropical-Like Cyclone to Physical Parameterizations. Atmosphere, 9(11), 436. https://doi.org/10.3390/atmos9110436, 2018.

Reale, O., and Atlas, R.: Tropical Cyclone–Like Vortices in the Extratropics: Observational Evidence and Synoptic Analysis. Wea. Forecasting, 16, 7–34, https://doi.org/10.1175/1520-0434(2001)016<0007:TCLVIT>2.0.CO;2, 2001.

Richardson I.G. and Cane H.V.: Near-Earth Interplanetary Coronal Mass Ejections During Solar Cycle 23 (1996--2009): Catalog and Summary of Properties, Sol. Phys. 264, 189–237, 2010. https://doi.org/10.1007/s11207-010-9568-6

Rodgers, E.B., Olson, W.S., et al., 1998. Satellite-Derived Latent Heating Distribution and Environmental Influences in Hurricane Opal (1995). Mon. Weather Rev. 126 (5), 1229–1247.

Rodgers, E., Olson, W., Halverson, J., Simpson, J., Pierce, H., 2000. Environmental forcing of Supertyphoon Paka's (1997) latent heat structure. J. Appl. Meteorol. 39, 1983–2006. https://doi.org/10.1175/1520-0450(2001)040<1983:EFOSPS>2.0.CO;2

Rogers, R. F., and Coauthors: Rewriting the Tropical Record Books: The Extraordinary Intensification of Hurricane Patricia (2015). Bull. Amer. Meteor. Soc., 98, 2091–2112, https://doi.org/10.1175/BAMS-D-16-0039.1. 2004.

Steranka, J., Rodgers, E. B., and Gentry, R. C.: The relationship between satellite-measured convective bursts and tropical cyclone intensification. Mon. Wea. Rev., 114, 1539– 1546, 1986.

Smith, E. J. and Wolfe, J. H.: Observations of interaction regions and corotating shocks between one and five AU: Pioneers 10 and 11, Geophys. Res. Lett., 3, 137–140, https://doi.org/10.1029/GL003i003p00137, 1976.

Tous, M. and Romero, R.: Meteorological environments associated with medicane development. Int. J. Climatol., 33: 1-14. https://doi.org/10.1002/joc.3428, 2013.

https://doi.org/10.5194/egusphere-2026-2327
Preprint. Discussion started: 1 June 2026

Trattner, K. J., Onsager, T. G., Petrinec, S. M. and Fuselier, S. A.: Distinguishing between pulsed and continuous reconnection at the dayside magnetopause, J. Geophys. Res. Space Physics, 120, 1684–1696, doi:10.1002/ 2014JA020713, 2015.

Tsurutani, B. T., Gonzalez, W. D., Gonzalez, A. L. C., Tang, F., Arballo, J. K., and Okada, M.: Interplanetary origin of geomagnetic activity in the declining phase of the solar cycle, J. Geophys. Res.-Space, 100, 21717–21733, https://doi.org/10.1029/95ja01476, 1995.

Tsurutani, B. T., Gonzalez, W. D., Gonzalez, A. L. C., Guarnieri, F. L., Gopalswamy, N., Grande, M., Kamide, Y., Kasahara, Y., Lu, G., Mann, I., McPherron, R., Soraas, F., and Vasyliunas, V.:: Corotating solar wind streams and recurrent geomagnetic activity: A review, J. Geophys. Res., 111, A07S01, https://doi.org/10.1029/2005JA011273, 2006.

Tsurutani, B. T., Lakhina, G. S., Sen, A., Hellinger, P., Glassmeier, K.-H., and Mannucci, A. J.: A review of Alfvénic turbulence in high-speed solar wind streams: Hints from cometary plasma turbulence, J. Geophys. Res.-Space, 123, 2458–2492, https://doi.org/10.1002/2017JA024203, 2018.

Yu, Jiaqi, Si Gao, Ling Zhang, Xinyong Shen, and Luyan Guo.: "Analysis of A Remote Rainstorm in the Yangtze River Delta Region Caused by Typhoon Mangkhut (2018)" Journal of Marine Science and Engineering 8, no. 5: 345. https://doi.org/10.3390/jmse8050345, 2020.